ORNL/CP-98993

BOREON STRENGTHENING IN FeAl

CONF-981054--

I. Baker*, X. Li*, H. Xiao*, O. Klein*, C. Nelson*, R. L. Carleton† and E. P. George†

* Thayer School of Engineering, Dartmouth College, Hanover, NH 03755.

† Metals and Ceramics Division, Oak Ridge National Laboratory, Oak Ridge, TN 37831.

ABSTRACT

The effect of boron on the strength of B2-structured FeAl is considered as a function of composition, grain size and temperature. Boron does not affect the concentrations of anti-site atoms or vacancies present, with the former increasing and the latter decreasing with increasing deviation from the stoichiometric composition. When vacancies are absent, the strength increase per at. % B per unit lattice strain, $\Delta\sigma/(\Delta c \times \varepsilon)$ increases with increasing aluminum concentration, but when vacancies are present (> 45 at. % Al), $\Delta\sigma/(\Delta c \times \varepsilon)$ decreases again. Boron increases grain size strengthening in FeAl. B strengthening is roughly independent of temperature up to the yield strength peak but above the point, when diffusion-assisted deformation occurs, boron strengthening increases dramatically.

DISCLAIMER

Introduction

Boron has been added to many intermetallic compounds and for several it not only increases their strength but also, in some cases, improves their low temperature ductility (1-5). However, this can be at the expense of the elevated temperature ductility (6). This paper is concerned with the effect of boron on the strength of FeAl. FeAl adopts the B2 or ordered body-centered cubic crystal structure, and, at least up to ~0.4Tm, deforms by the glide of pairs of antiphase boundary-coupled a/2<111> dislocations (7), see Figure 1.

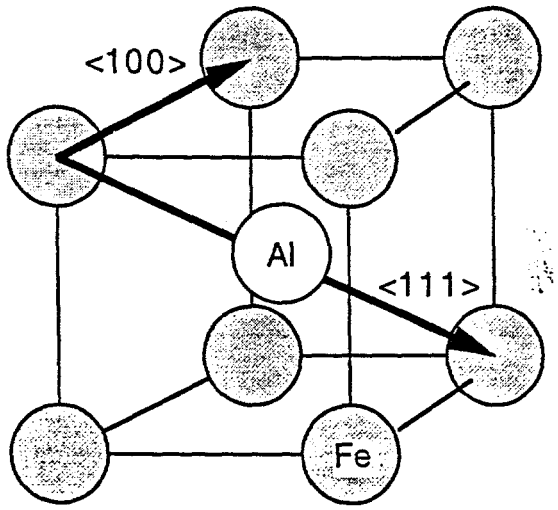

Figure 1. The B2 structure adopted by FeAl, showing the <111> and <100> slip vectors.

Solubility of Boron

Recent hard-sphere modeling of interstitial sites in B2 compounds (8) has indicated that the tetrahedral site is always the largest interstitial site, irrespective of the size of the constituent atoms. Thus, it is likely that the boron occupies the tetrahedral interstitial sites. The exact solubility of boron in FeAl is not known. Iron borides have been in several studies, but it is not clear whether the solubility limited was exceeded or whether the boron was not evenly distributed throughout the alloy. Gaydosh *et al.* (9) found mostly spherical (but occasionally plate-like) body-centered tetragonal Fe_2B boride particles in a range of boron-doped (0.41 at. %) alloys based on a nominal composition of Fe-40Al which also contained small additions of either carbon, zirconium or hafnium. Munroe and Baker (10) noted the presence of boride needles in boron-doped (0.05 at. %) Fe-45Al, although they were not evenly distributed in all grains. Similarly, Pierron and Baker (11) found both spherical and needle-like borides sparsely distributed in both Fe-43Al and Fe-48Al containing 0.12 at. % B. However, in the latter case the precipitates were found to have a previously-unreported tetragonal crystal structure with a strong orientation relationship with the B2 matrix, i.e. $(001)_{B2} \parallel (001)_T$; $[100]_{B2} \parallel [100]_T$.

Lattice Strengthening

Several workers (12-17) have shown that boron additions increase the room-temperature yield strength of FeAl. However, it is difficult to obtain the magnitude of the boron strengthening from these studies since the alloys were not all given the same heat-treatments. Thus, they may have had different vacancy concentrations and different grain sizes, both of which affect the yield strength. To study its intrinsic behavior, it is necessary to give FeAl a low temperature anneal, typically 5 days at 673K (18), in order to remove the vacancies retained after a high temperature anneal. It is also necessary to use large grain sizes to circumvent the substantial grain boundary strengthening observed in these materials (19). It is not sufficient to compare materials at the same (small) grain size since the contribution from grain boundary strengthening is changed by alloying i.e. k is changed in the Hall-Petch relationship

$$\sigma_y = \sigma_o + kd^{-\frac{1}{2}} \qquad (1)$$

where σ_y is the yield strength, σ_o is the lattice resistance, and d is the grain size.

Grain-Size Strengthening

Pike and Liu (20) demonstrated that boron increases k for Fe-40Al from near-zero (-69 MPa $\mu m^{0.5}$) to 534 MPa $\mu m^{0.5}$, but σ_0 is essentially unchanged at 350 MPa. Gaydosh *et al.* (9) obtained values of 342 MPa and 462 MPa $\mu m^{0.5}$ for σ_0 and k, respectively, for Fe-40Al, as opposed to values of 199 MPa and 720 MPa $\mu m^{0.5}$ obtained by Baker *et al.* (19). These differences in σ_o and k for Fe-40Al probably largely reflect differences in heat-treatment, *viz.*, Gaydosh *et al.* (9) annealed their material at 1100 K for two hours followed by a furnace cool whereas Baker *et al.* (19) gave their material a low temperature anneal of 120 h at 673 K after high temperature grain growth anneals. Interestingly, comparison of the results of Baker *et al.* (19) and Gaydosh *et al.* (9) suggests that an increased vacancy concentration decreases the value of k, possibly because the lattice resistance of fine-grained material is less affected by retained vacancies than large-grained material (since there is a greater density of sinks for the vacancies). The large-grained specimens studied by Pike and Liu (20) were annealed at high temperature, followed by two hours at 973 K and then one day at 573 K – the latter anneal has little effect on the vacancy concentration due to the low vacancy mobility at that temperature (21) – whilst the fine-grained specimens were annealed at temperatures from 893 K to 973 K and so probably had lower vacancy concentrations.

Similar to the result reported by Pike and Liu (20) for Fe-40Al, near-zero values of k have been reported for the B2 compounds AuZn (22,23) and NiAl (19-24) at their stoichiometric compositions. In the latter compound, slip is wavy (19) and cross-slip is easy at the

stoichiometric composition and, thus, a cell structure forms at very low strains (25,26). Thus, the dislocations do not probe the grain boundaries. In contrast, slip in FeAl is planar (19).

Since the different heat treatments used by Pike and Liu (20) on different specimens could have affected the results, Li and Baker (27) studied the effect of boron on the Hall-Petch slope of Fe-45Al, given a vacancy-reducing anneal of 118 hrs at 673K (18). They found a very similar result to that of Pike and Liu (20), i.e., boron increased k from 544 MPa $\mu m^{0.5}$ to 1766 MPa $\mu m^{0.5}$, see Figure 2. Again, σ_o was similar (166 MPa) with and without boron.

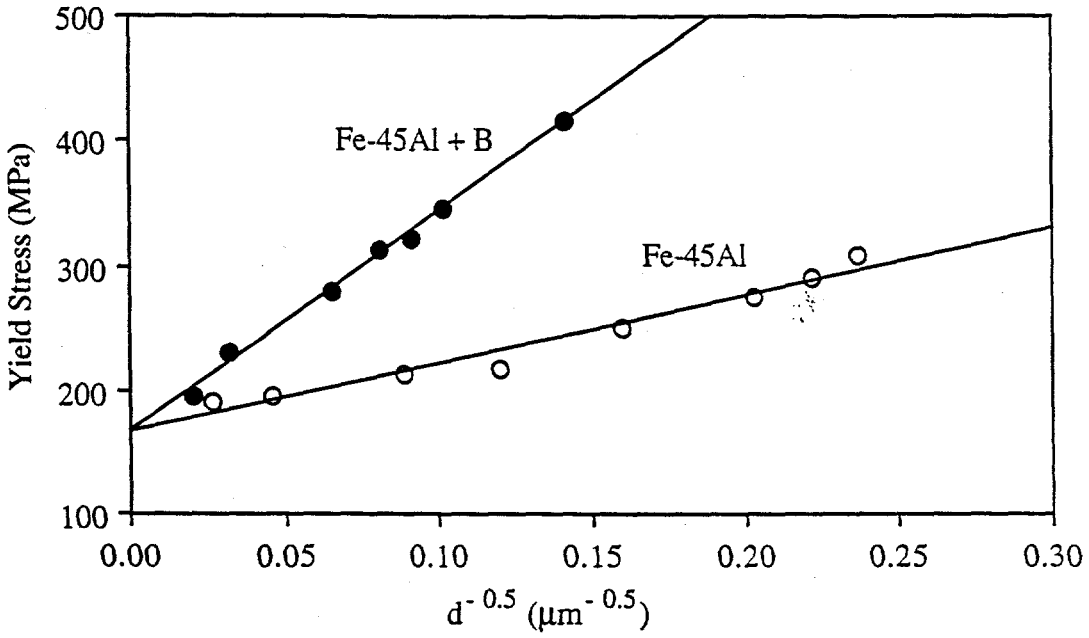

Figure 2. Room temperature yield stress (0.2% offset stress) as a function of (grain size)$^{-0.5}$ for Fe-45Al with and without 0.05 at. % boron (27).

The results of Pike and Liu (20) and Li and Baker (27) are intriguing. They suggest that boron has no strengthening effect in the lattice but that boron, which is known to segregate to the grain boundaries (28), increases the difficulty of slip transmission across grain boundaries. The latter effect is contrary to that observed when boron is added to the nickel-based ordered face-centered cubic ($L1_2$) compounds Ni_3Al (29), Ni_3Si (30), Ni_3Ge (31) and Ni_3Ga(32), where it reduces k.

The Effect of Boron on the Yield Anomaly

At around 0.4 Tm, FeAl shows a yield strength peak whose exact magnitude and temperature depend on composition, strain rate and, for single crystals, both orientation and sign of the applied stress, see reference 33 for a review. Studies on large-grained FeAl by Klein and Baker (34), heat-treated to remove excess thermal vacancies, demonstrated that the addition of 0.05 at. % B to Fe-45Al shifts the yield strength peak to both higher temperature and to a higher stress, Figure 3. Carleton *et al.* (35) found that boron-doped (0.03 at. %) polycrystalline FeAl

containing from 40 to 48 Al showed similar behavior to undoped alloys (36), but that the yield strength peaks in the boron-doped alloys occurred at higher temperatures (~833 K) than in the equivalent undoped alloys (~675 K), although significantly the boron-doped alloys were tested at a faster strain rate. Guo *et al.* (37) also observed yield stress peaks in several cast Fe-38Al alloys doped with either boron or boron and zirconium. The peaks they observed occurred at ~893 K, an even higher temperature than that observed by Carleton *et al.* (35), but they did not specify the strain rate at which testing was performed.

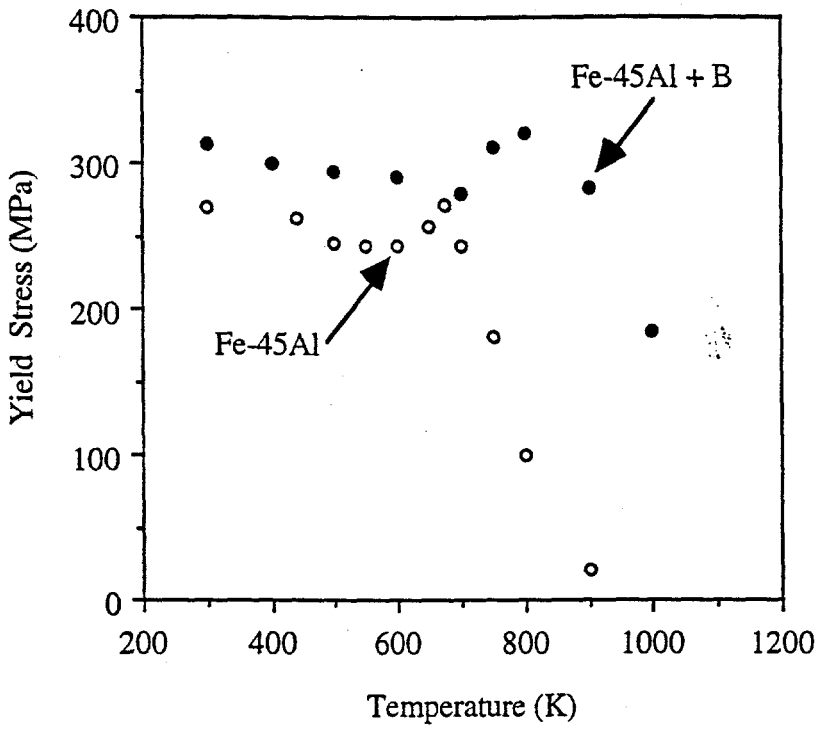

FIGURE 3. Graph of yield strength versus temperature for large-grained, low-temperature-annealed Fe-45Al and Fe-45Al + B strained under tension at $1x10^{-4}s^{-1}$ (34).

It is possible to estimate the magnitude of the boron strengthening as a function of temperature by comparing the yield strengths of large-grained, low-temperature-annealed Fe-45Al and Fe-45Al + 0.05 B (34). Figure 4 shows the results as the strength increase per atomic percent boron as a function of temperature. It is evident that between 300 K and 700 K (the latter is approximately the temperature of the anomalous yield stress peak), the boron strengthening effect is almost independent of temperature at ~0.72-1.0 GPa per atomic percent boron. Above 700 K, where diffusion-assisted deformation starts to operate, boron strengthens Fe-45Al much more dramatically, see Figure 4.

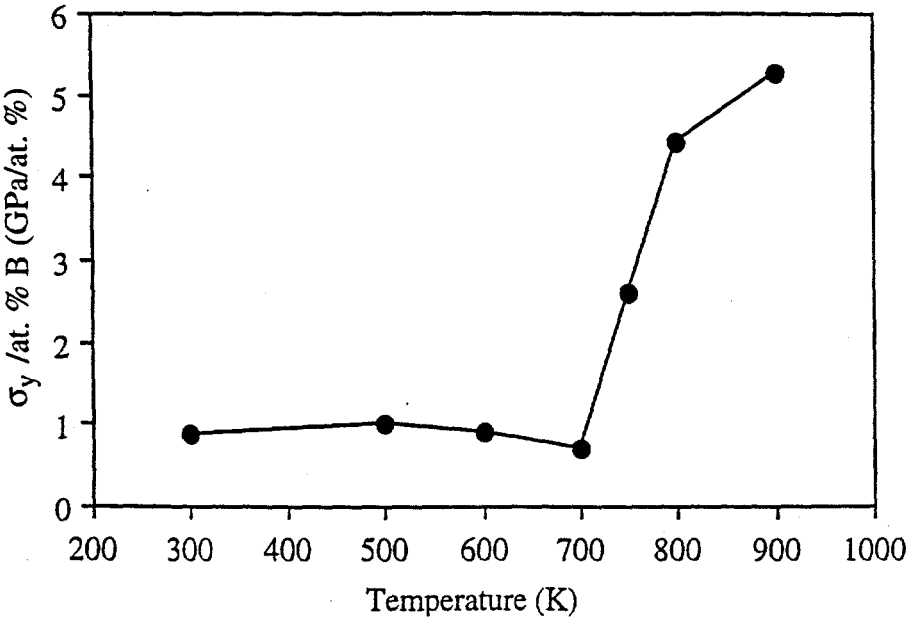

Figure 4. Yield strength increase per atomic percent boron for large-grained, low-temperature annealed Fe-45Al as a function of temperature. From the data in reference 34.

Effect of Boron on the Concentrations of Vacancies and Anti-site Atoms

Boron, unlike substitutional elements in FeAl (38), appears to accelerate the rate at which the equilibrium vacancy concentrations are re-established during low temperature annealing (39), after annealing at elevated temperature.

In order to determine if boron affects the vacancy concentrations and anti-site atom concentrations in FeAl, the relative integrated x-ray intensities were measured from powders ground from FeAl alloys containing 40, 43 45, 48 and 50 at. % Al both with and without boron (0.12 at. % B) using a Siemens D5000 x-ray diffractometer equipped with a Kevex solid state detector, details are given elsewhere (40). For each alloy, three separate measurements were made using Cu radiation, with the powder unloaded and reloaded between measurements and the three results averaged.

The calculated relative integrated intensities for the {100} superlattice and {200} fundamental reflections are given by

$$\left\{\frac{I_{(100)}}{I_{(200)}}\right\}_{(cal.)} = \frac{\left\{\left(\frac{1+\cos^2 2\theta}{\sin^2\theta\cos\theta}\right)e^{-2M}\left|F_s\right|^2\right\}_{(100)}}{\left\{\left(\frac{1+\cos^2 2\theta}{\sin^2\theta\cos\theta}\right)e^{-2M}\left|F_f\right|^2\right\}_{(200)}} \qquad (2)$$

where F is the structure factor, $(1 + \cos^2 2\theta)/(\sin^2\theta.\cos\theta)$ is the Lorentz-polarization factor, for the appropriate Bragg angle, θ, and e^{-2M} is the temperature factor. M is given by

$$M = B(\sin\theta / \lambda)^2 \tag{3}$$

where λ is the x-ray wavelength, and B is obtained experimentally, as described elsewhere (40). The structure factor for the (200) fundamental reflection can be written (40):

$$F_f = \frac{X_{Fe}}{X_{Al}}(1 - Y_{Fe/Al})f_{Fe} + (1 - Y_{Fe/Al})f_{Al} \tag{4}$$

and that for the (100) superlattice reflection as

$$F_s = \left[\frac{X_{Fe}}{X_{Al}}(1 - Y_{Fe/Al}) - 2Y_{Fe/Al} \right] f_{Fe} - (1 - Y_{Fe/Al})f_{Al} \tag{5}$$

Where f_{Al} and f_{Fe} are the atomic scattering factors for Al and Fe, respectively; $Y_{Fe/Al}$ is the fraction of Fe atoms that occupy Al sites, and X_{Fe} and X_{Al} are the atomic fractions of Fe and Al in the alloy, respectively.

By comparing the observed and calculated values of $I_{(100)}/I_{(200)}$, the measured long range order parameter, S, can be obtained from

$$S_{meas} = \sqrt{\frac{I_{(100)} / I_{(200)}(obs.)}{I_{(100)} / I_{(200)}(cal.)}} \tag{6}$$

where $I_{(100)}/I_{(200)}$(cal.) in this case is calculated assuming no vacancies are present and that excess Fe atoms substitute on the other (aluminum) sublattice site but that there are no other anti-site atoms than these. The maximum degree of order is given by $S_{Al}^{max} = 2X_{Al}$. For the stoichiometric composition, maximum order means that there are no vacancies present and all Fe and Al atoms occupy their own sites. For iron-rich FeAl, maximum order means that no vacancies exist and the excess Fe atoms substitute on the other (aluminum) sublattice site.

Table 1 compares the measured long-range order parameter, S_{meas}, with the calculated maximum value, S_{Al}^{max}. Within experimental error, the values for boron-doped and undoped FeAl are the same. The measured values for the alloys containing few vacancies (40 - 45 at. % Al) are very close to the theoretical values, suggesting that sample granularity effects on the x-ray intensities arising from the large particle size was not significant (41).

Table I. Comparison of the measured long range order parameter, S_{meas}, with the calculated maximum possible value, S_{Al}^{max}, for boron-doped FeAl alloys. The ± indicates the largest deviation of three measurements.

Composition	Fe-40	Fe-43Al	Fe-45Al	Fe-48Al	Fe-50Al
S_{Al}^{max}	0.80	0.86	0.90	0.96	1.00
S_{meas} (B-free)	0.79±0.02	0.85±0.02	0.91±0.01	0.94±0.01	0.94±0.02
S_{meas} B-doped	0.79±0.03	0.85±0.03	0.89±0.03	0.94±0.03	0.96±0.03

When $S_{meas} \approx S_{Al}^{max}$, maximum order is achieved and no constitutional vacancies are present. If $S_{meas} < S_{Al}^{max}$, $Y_{Fe/Al}$ can be calculated, using the structure factor equations above, by comparing the calculated and measured values of $I_{(100)}/I_{(200)}$. Having calculated $Y_{Fe/Al}$, the fractions of Fe atoms that occupy the Fe-sites, $Y_{Fe/Fe}$ can be obtained from (40):

$$Y_{Fe/Fe} = \frac{X_{Fe}}{X_{Al}}\left(1 - Y_{Fe/Al}\right) - Y_{Fe/Al} \qquad (7)$$

and the fraction of vacancies that occupy Fe sites, $Y_{v/Fe}$ and the fraction of Al atoms that occupy Al sites $Y_{Al/Al}$ can be calculated from

$$Y_{Fe/Fe} + Y_{V/Fe} = Y_{Al/Al} + Y_{Fe/Al} = 1 \qquad (8)$$

The measured concentration of Fe anti-site atoms on the aluminum sub-lattice and vacancies on iron sites as a function of atomic percent aluminum for FeAl with and without boron are shown in Figure 5. Note that the concentrations of Al anti-site atoms on the iron sub-lattice and vacancies on the aluminum sites were assumed to be zero. There are some x-ray data which indicate that perhaps 6% of the Fe sub-lattice sites are occupied by Al irrespective of the Fe:Al ratio (42), although in that study the vacancy concentrations were assumed to be zero. Thus, the anti-site atom concentrations may be somewhat higher than indicated in Figure 5, but, within experimental error, the data for unalloyed and boron-doped FeAl are similar. The vacancy concentrations are low from 40 to 45 at. % Al but then increase towards the stoichiometric composition, and the anti-site atom concentrations increase approximately linearly with increasing deviation from the stoichiometric composition.

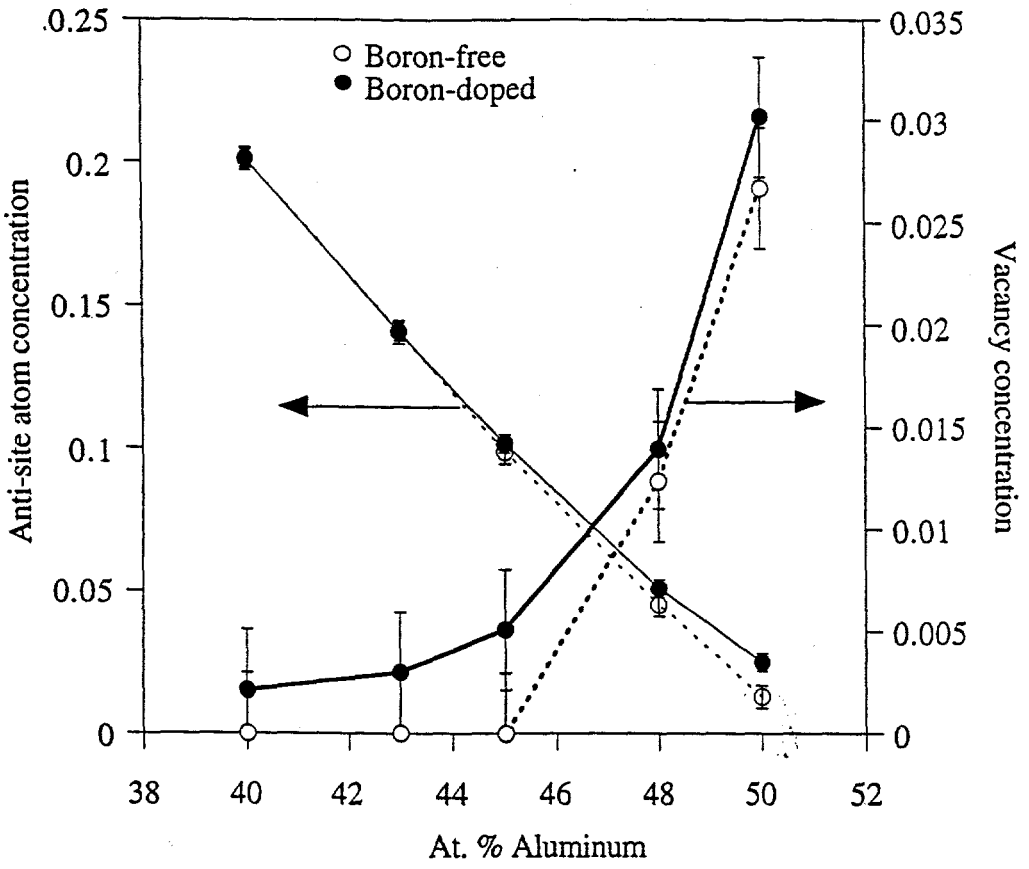

Figure 5. Concentrations of Fe anti-site atoms on the aluminum sublattice, $Y_{Fe/Al}$, and vacancies on the iron sublattice, $Y_{V/Fe}$, as a function of aluminum concentration.

Lattice Strain

In order to relate the strengthening due to boron to the lattice strain, compression tests were performed on five large-grained (250-300 μm), low-temperature-annealed (5 days at 673 K) FeAl alloys (40, 43 45, 48 and 50 at. % Al) both with and without boron (0.12 at. % B) in air at an initial strain rate of ~1 x 10^{-4} s^{-1}. To determine the lattice strain, lattice parameter measurements were made on powders filed from each alloy, ground, to reduce the particle size, sieved to -400 mesh (< 25 μm), annealed in argon for one hour at 1073 K, furnace-cooled, and re-annealed at 673 K for 120 hours. The exact values of the lattice parameters were determined, using the Debye-Scherrer x-ray method with Ni-filtered Cu K_α radiation and the Nelson-Riley extrapolation method (44), to an accuracy of $\pm 2 \times 10^{-5}$ nm, as described in detail elsewhere (40,43). Three lattice parameter measurements were made on each alloy and the results averaged.

Figure 6 shows both the increase in lattice parameter, Δa, per unit increase in boron concentration, Δc, and the lattice strain, ε, = $100\Delta a/\Delta c \times a_o$, as a function of atomic percent aluminum. The increase in lattice parameter indicates that the boron atoms, which are smaller than either the iron or aluminum atoms, occupy the tetrahedral interstitial sites. In Figure 6, it is evident that the lattice strain due to boron decreases with increasing aluminum concentration. The

change in the slope of both curves on Figure 6 above 45 at. % Al corresponds to the occurrence of vacancies in the material, as indicated in Figure 5.

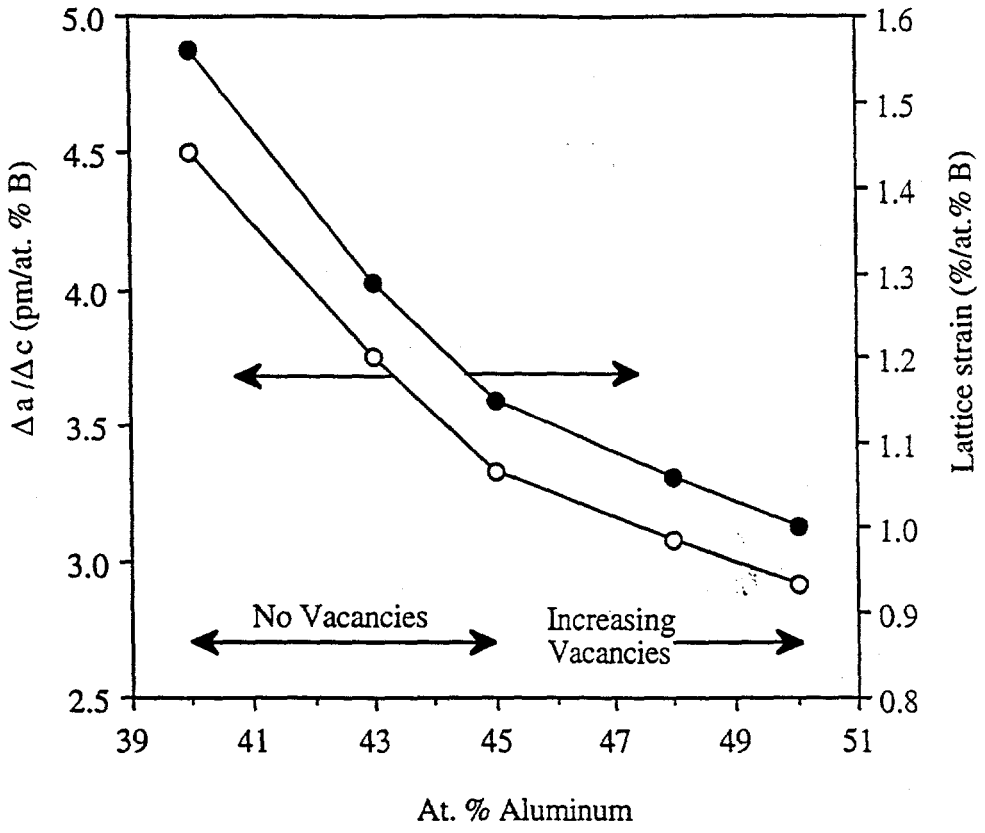

Figure 6. Change in lattice parameter per unit change in the concentration of boron, $\Delta a/\Delta c$, and percentage change in lattice strain as a function of atomic percent aluminum.

The yield stress is shown as a function of atomic percent aluminum for both unalloyed and boron-doped FeAl in Figure 7. It is evident that boron produces an increase in yield strength, $\Delta\sigma_y$, at all aluminum concentrations. Also shown on Figure 7 is the increase in yield strength per atomic percent boron, $\Delta\sigma/\Delta c$, as a function of aluminum concentration. It is worth noting that the yield strength of similarly-processed Fe-45Al doped with only 0.05 at. % boron has been measured to be 313 MPa (45), producing a value of $\Delta\sigma/\Delta c$ of 860 MPa/at. % B, which is very similar to the value of 890 MPa/at. % B obtained for the Fe-45Al containing 0.12 at. % B measured here. This tends to suggest both a linear relationship between the yield strength and the boron concentration and that the majority of the boron in the alloys was in solution. It is evident in Figure 7 that in the absence of vacancies, i.e. from 40 to 45 at. % Al, the strengthening effect of boron increases with increasing aluminum concentration. However, once vacancies are present, i.e. in 48 and 50 at. % Al, the strengthening effect decreases. This suggests that the boron atoms are associated with vacancies, i.e. the strain fields due to the lattice expansion from the boron is accommodated by associating with vacancies. An association between vacancies and boron atoms was by Gay *et al.* (39). However, this association appears to be inconsistent with the reported increase in vacancy

migration rate in FeAl, which produces a decrease in annealing time to reach the equilibrium vacancy concentration, when boron is present (39).

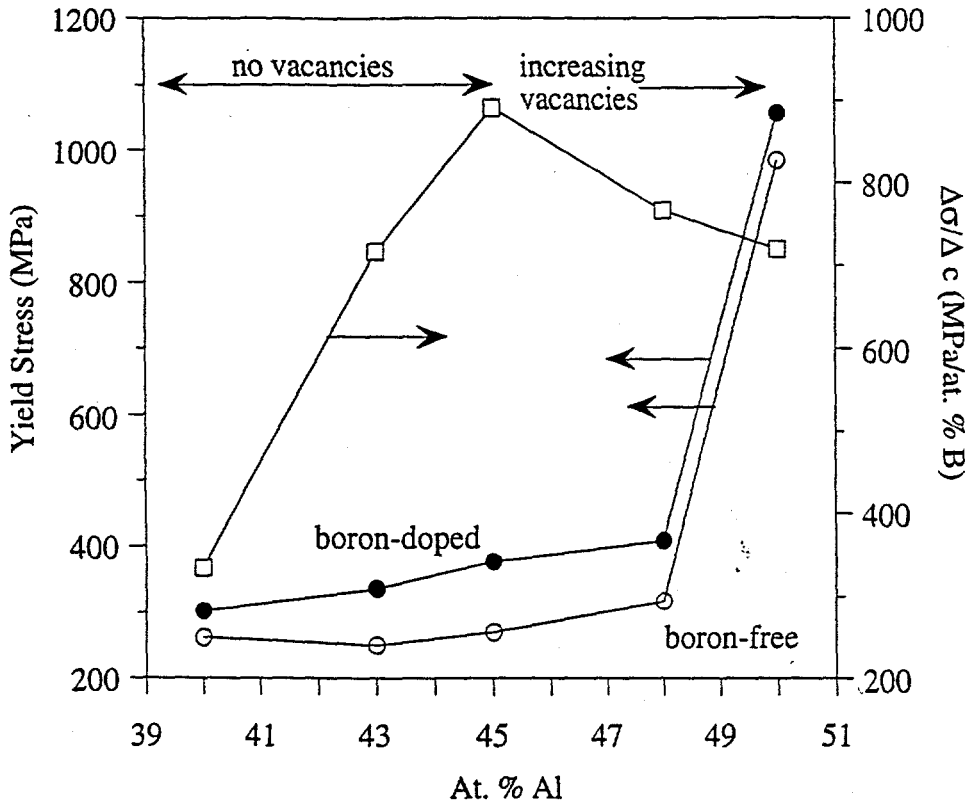

Figure 7. Graph of the yield strength of large-grained, low temperature annealed boron-doped and unalloyed FeAl, and the increase in yield stress per unit increase in boron concentration, $\Delta\sigma/\Delta c$, as a function of atomic percent aluminum.

Data from Figures 6 and 7 are replotted in Figure 8 as $\Delta\sigma/(\Delta c \times \varepsilon)$ or equivalently $\Delta\sigma/(\Delta a/a_0)$, as a function of atomic percent aluminum. The data are plotted on the left hand ordinate in terms of their absolute values and on the right hand ordinate normalized with respect to the shear modulus, G(26), assuming a Poisson's ratio of 1/3.

With the data in the form shown in Figure 8 it is evident that even though the lattice strain decreases with increasing aluminum (Figure 6), this is more than offset by the increasing strength with increasing aluminum for alloys containing from 40-45 at. % Al. In other words, the data (for 40-45 at. % Al) show that the lattice strain alone does not control the strengthening due to boron (otherwise $\Delta\sigma_y/(\Delta c \times \varepsilon)$ would be independent of aluminum concentration). Instead, the results indicate that there is chemical dependence to the boron strengthening, i.e. boron strengthening is greater if more aluminum is present. One may speculate that this increased strengthening manifests itself physically through boron's association with the anti-phase boundaries, APBs, between the gliding paired $\frac{a}{2}\langle 111\rangle$ dislocations, see references 47 and 48.

Based on hard-sphere modelling, interstitial sites are larger at the APB (8). Since, the APB energy increases with increasing aluminum concentration in FeAl (49), there may be a tendency for boron atoms to segregate to the APB and to lower its energy with increasing aluminum concentration. This increased segregation to the APB, will cause a greater drag on gliding APB-coupled dislocations and, hence, lead to an increase in strength. This trend would also presumably continue for alloys containing 48 and 50 at. % aluminum except that the vacancies present in some way offset this. Perhaps, the strain fields from the boron are ameliorated by the vacancies.

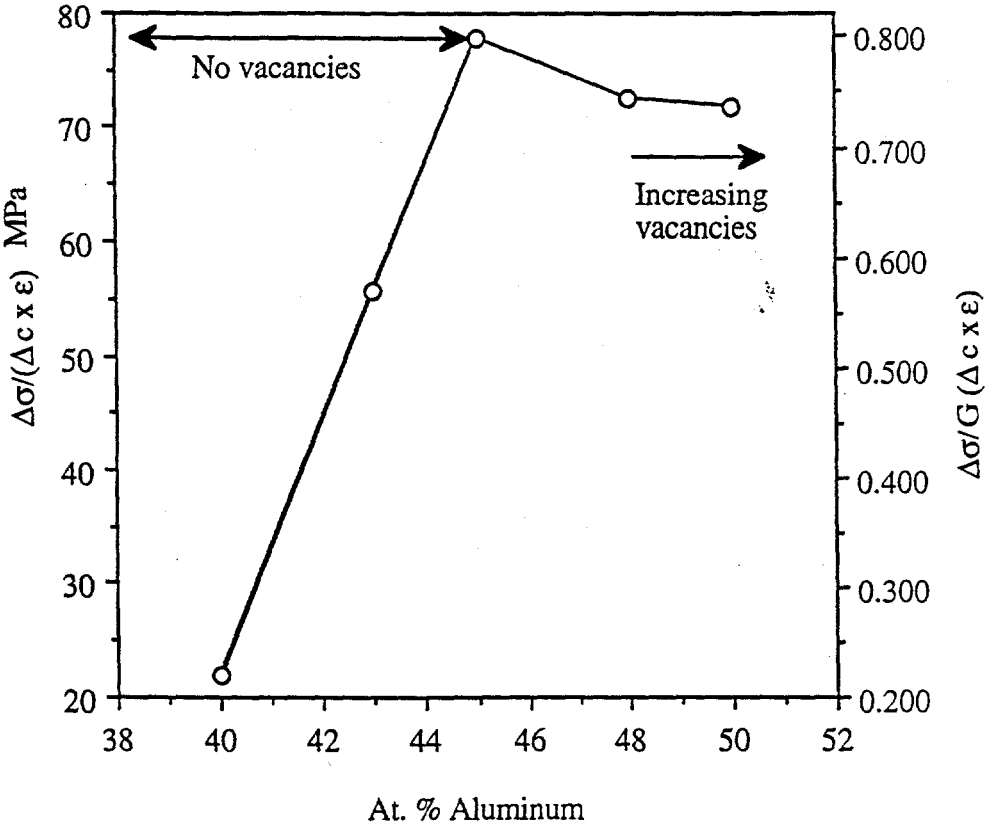

Figure 8. Strength increase per atomic percent boron per unit lattice strain, $\Delta\sigma/(\Delta c \times \varepsilon)$ or strength increase per fractional change in lattice parameter as a function of atomic percent aluminum. The left hand ordinate shows the absolute value and the right hand ordinate shows the value normalized with respect to the shear modulus (46).

Finally, the strengthening per fractional increase in lattice parameter, $\Delta\sigma/(\Delta c \times \varepsilon)$, of FeAl due to boron is in the range 0.23G - 0.83G. This is substantially greater than the boron strengthening effect in Ni-based $L1_2$ compounds i.e., $\Delta\sigma/(\Delta c \times \varepsilon) = 0.04G$, for Ni_3Al [29,30,50] and Ni_3Ga [5], 0.05G for Ni_3Si [31] and 0.06G for Ni_3Ge [32]. The greater strengthening in FeAl presumably reflects the smaller interstitial sites available in B2 compounds than in $L1_2$ compounds.

Conclusions

An analysis of the data on boron strengthening in FeAl has shown that:

1. Boron does not affect the degree of order, vacancy concentration or anti-site atom concentration in FeAl.

2. Boron increases the Hall-Petch Slope.

3. Boron increases the temperature and magnitude of the yield stress peak in FeAl.

4. The strengthening effect of boron in FeAl is roughly independent of temperature from 300K to 700K, above which it rises rapidly.

5. The compositional dependence of the effect of boron on the strength of FeAl depends on whether vacancies are present: for FeAl containing few vacancies ($\leq$ 45 at. % Al) the strength increase per atomic percent boron increases with increasing aluminum concentration; when vacancies are present ($\geq$ 48 at. % Al), boron strengthening shows little change with aluminum concentration, suggesting that the vacancies significantly interact with boron.

6. The strength increase due to boron per unit increase in lattice parameter at room temperature is 0.22G - 0.80G depending on the aluminum concentration, is an order of magnitude greater than the boron strengthening of nickel-based $L1_2$ compounds.

Acknowledgments

This work was supported by the U.S. Department of Energy, Office of Basic Energy Sciences, Division of Materials Sciences through contract number DE-FG02-87ER45311 with Dartmouth College, contract DE-AC05-96OR22464 with Lockheed Martin Energy Research Corporation, and through the SHaRE program under contract DE-AC05-76OR00033 with the Oak Ridge Associated Universities.

References

1. K. Aoki and O. Izumi, Nippon Kinzoku Gakkaishi, 43 (1979), 1190.
2. C.T. Liu, C.L. White, and J.A. Horton, Acta Metall., 33 (1985), 213 .
3. W.C. Oliver and C.L. White, MRS symp. proc. on High Temperature Ordered Intermetallic Alloys II, 83 (1987), 241.
4. A.I. Taub and C.L. Briant, Metall. Trans., 20 (A) (1989), 2025.
5. X. Yu and E.M. Schulson, Acta Metall. Mater., 43 (1995), 2121.

6. I. Baker, O. Klein, C. Nelson, and E.P. George, Scripta Metall. Mater., 30 (1994), 863-868.
7. B.K. Kad and J.A. Horton: Mater. Sci. Eng., (1997) (in press).
8. I. Baker, Journal of Materials Research, 8 (1993), 1203.
9. D.J. Gaydosh, S.L. Draper, and M.V. Nathal: Metall. Trans. 20A (A) (1989), 1701-1714.
10. P.R. Munroe and I. Baker: Phil. Mag. 72 (A) (1995), 1301-1310.
11. Pierron and I. Baker, High Temperature Ordered Intermetallic Alloys VII, eds. C.C.Koch et al., (Pittsburgh, PA: Materials Research Society, 1997), 460, 331 - 336.
12. M.A. Crimp, K. Vedula, and D.J. Gaydosh: in High Temperature Ordered Intermetallic Alloys II, eds. N.S. Stoloff et al., (Pittsburgh, PA, Materials Research Society, 1987), 81, 499-504.
13. R.J. Lynch and L. A. Heldt: Scripta Metall. Mater., 30 (1994), 895-898.
14. M.A. Crimp and K.M. Vedula: Mater. Sci. Eng., 165 (A) (1993), 29-34.
15. O. Klein and I. Baker: Scripta Metall. Mater., 27 (1992), 1823-1828.
16. C.T. Liu and E.P. George: in High Temperature Ordered Intermetallic Alloys IV, eds. L.A. Johnson et al., (Pittsburgh, PA, Materials Research Society, 1991) 213, 527-532.
17. M.A. Crimp and K. Vedula: Mater. Sci. Eng., 78 (1986), 193-200.
18. P. Nagpal and I. Baker, Metallurgical Transactions, 21 (A) (1990), 2281.
19. I. Baker, P. Nagpal, F. Liu and P.R. Munroe, Acta Metall. Mater., 39 (1991), 1637.
20. L.M. Pike and C. T. Liu: Scripta Metall. Mater., 25 (1991), 2757-2761.
21. D. Weber, M. Meurtin, D. Paris, A. Fourdeaux, and P. Lesbats: J. de Phys. 38 (C7) (1977), 332-336.
22. A.R. Causey and E. Teghtsoonian, Metall. Trans. 1A (1970), 1177.
23. A. Causey, (Ph.D. Thesis, University of British Columbia 1968).
24. P. Nagpal and I. Baker, Scripta Metall., 24 (1990), 2381
25. P. Nagpal and I. Baker, J. Mater. Sci. Lett., 11 (1992), 1209.
26. P. Nagpal, I. Baker and J.A. Horton, Intermetallics, 2 (1994), 23.
27. X. Li and I. Baker: Scripta Metall. Mater., 34 (1996), 1219-1223.
28. C.T. Liu and E.P. George: Scripta Metall. Mater., 24 (1990), 1285-1290.
29. E.M. Schulson, T.P. Weihs, I. Baker, H.J. Frost, and J.A. Horton: Acta Metall., 34 (1986), 1395-1399.
30. E.M. Schulson, Y. Xu, P.R. Munroe, S. Guha and I. Baker, Acta Metall. Mater., 39 (1991), 2971.
31. E.M. Shulson, L.J. Briggs and I. Baker, Acta Metall. Mater., 38 (1990), 207.
32. J. Fang and E.M. Schulson, Mater. Sci. Eng., A152 (1992), 138.
33. I. Baker and P.R. Munroe, Int. Mater. Rev., (in press).
34. O. Klein and I. Baker: Scripta Metall. Mater., 30 (1994), 627-632.
35. R. Carleton, E.P. George, and R.H. Zee: Intermetallics, 3 (1995), 433-441.

36. I. Baker, H. Xiao, O. Klein, C. Nelson, and J.D. Whittenberger: Acta Metall. Mater., 43 (1995), 1723-1730.
37. J.T. Guo, O. Jin, W.M. Yin, and T.M. Wang: Scripta Metall. Mater., 29 (1993), 783-785.
38. J.H. Schneibel, P.R. Munroe, and L. Pike, High Temperature Ordered Intermetallic Alloys VII, eds. C.C.Koch et al., (Pittsburgh, PA, Materials Research Society, 1997), 460, 379-384.
39. A.S. Gay, A. Frackiewicz, and M. Biscondi: J. de Physique IV, 6 C2 (1996), 153-158.
40. I. Baker, X. Li, H. Xiao, R.L. Carlton and E. P. George, Intermetallics, 6 (1998), 177-183.
41. C.J. Sparks, R. Kumar, E.D. Specht, P. Zschack, G.E. Ice, T. Shiraishi and K. Hisatsune, Advances in X-ray Analysis, Ed. - C.S. Barrett et al., (Plenum Press, NY, 1992), 57.
42. S. Khosla, C.J. Sparks, J. Schneibel, E.D. Specht, X. Jiang, M.K. Miller, P. Zschack and C.J McHargue, Proc Cong. on Alloy Modelling and Design, Eds. G.M. Stocks and P.E.A. Turchi, TMS Symposium, (Pittsburgh, 1993).
43. H. Xiao and I. Baker, Acta Metallurgica et Materialia, 43 (1995), 391.
44. B.D. Cullity, Elements of X-ray Diffraction, Second Edition, Addison-Wesley Publishing Company, Inc., (Reading, MA, 1978).
45. O. Klein and I. Baker, Scripta Metallurgica et Materialia, 27 (1992), 1823.
46. M.R. Harmouche and A. Wolfenden, Materials Science and Engineering, 84 (1986), 35.
47. I. Baker and P. Nagpal, in Structural Intermetallics, Edited by R. Darolia et al., The Metallurgical Society, (Warrendale, Pa., 1993), 463.
48. I. Baker, in Processing, Properties and Applications of Iron Aluminides, Edited by J.H. Schneibel and M.A. Crimp, The Metallurgical Society, (Warrendale, Pa., 1994), 101.
49. I. L. F. Ray, R. C. Crawford and D. J. H. Cockayne, Philosophical Magazine, 21 (1970), 1027.
50. I. Baker, B. Huang and E.M. Schulson, Acta Metallurgica, 36 (1988), 493.